Schweizerische Eidgenossenschaft
Confédération suisse
Confederazione Svizzera
Confederaziun svizra

Swiss Department for
Environment, Transport, Energy and Communications
Swiss Federal Office of Energy SFOE

Evaluation of Solar Thermal Storages with Quantitative Flow Visualisation

W. Logie, E. Frank and A. Luzzi

July 11, 2008

Institution	Institut für Solartechnik SPF HSR Hochschule für Technik Rapperswil
Address	Oberseestrasse10, CH-8640 Rapperswil
Telephone, Fax	+41 55 222 4821, +41 55 222 4844
E-mail, Website	info@solarenergy.ch, www.solarenergy.ch
BFE Project/Contract number	102340/152949
BFE Project director	Jean-Christophe Hadorn
Project runtime	01.10.2007 – 01.07.2008

Abstract

The non-intrusive Quantitative Flow Visualisation (QFV) Techniques of Particle Imaging Velocimetry (PIV) and Laser Induced Fluorescence (LIF) have been evaluated in the context of experimental investigations on solar Thermal Energy Storages (TES). Much competence and experience has been gained in the integration of these powerful yet complex and time consuming flow analysis methods into the realm of laboratory experimentation. In addition to gathering experience in the application of QFV techniques, a number of charging and discharging variations were considered in light of exergetic evaluation for the influence they have on the ability of a TES to stratify. The contemporary awareness that poorly chosen pitch to diameter ratios by the design of immersed coil heat exchangers leads to a reduction in heat exchange and an increase in mixing phenomenon has been confirmed. The observation of two combitank (combined hot water and heating) configurations has shown that free convective heat transfer forces in the form of mixing energy play a significant role in the stratification efficiency of thermal energy storages.

Contents

1 Motivation **1**

2 Aim **1**

3 Theory **1**
3.1 Balancing Entropy/Exergy in a Thermal Energy Storage (TES) 2

4 Method **3**
4.1 Quantitative Flow Visualisation (QFV) 4
4.1.1 Particle Imaging Velocimetry (PIV) 5
4.1.2 Laser Induced Fluorescence (LIF) 6
4.2 Charging of a TES with an Immersed Heat exchanger (IHX) 6
4.3 Discharging of Combitank Domestic Hot Water (DHW) 8

5 Results and Discussion **9**
5.1 Charging of TES with an IHX 9
5.2 Discharging of Combitank DHW 11

6 Conclusion and Outlook **22**

A Background **23**

B Imaging Velocimetry **23**
B.1 Planar Particle Imaging Velocimetry (PIV) 24

C Fluorescence Techniques **26**
C.1 Concentration measurements with PLIF 27
C.2 Temperature measurements with PLIF 28

D Exergy of TES **29**

NOMENCLATURE

d	tube diameter	$[m]$
L	coil length	$[m]$
H	coil height	$[m]$
p	coil pitch	$[m]$
D	helix coil diameter	$[m]$
A	surface area	$[m^2]$
V	volume	$[m^3]$
c	specific heat	$[kJ.kg^{-1}.K^{-1}]$
λ	thermal conductivity	$[W.m^{-1}.K^{-1}]$
T	temperature	$[K]$
Nu	nusselt number	
ε	heat exchanger effectiveness	
$\dot{v}$	volume flow rate	$[l/h]$
$\dot{m}$	mass flow rate	$[kg.s^{-1}]$
Q	heat transfer	$[J]$
$\dot{Q}$	heat transfer rate (power)	$[W]$
Θ_m	log mean temperature difference	
h	heat transfer coefficient	$[W.m^{-2}.K^{-1}]$
UA	heat transfer area coefficient	$[W.K^{-1}]$
S	entropy	$[J.K^{-1}]$
Ξ	exergy	$[J]$

Subscripts

hx	heat exchanger
in	inlet
out	outlet
i	inner
o	outer
tes	thermal energy storage
dhw	domestic hot water
1	beginning of charge/discharge (t_1)
2	end of charge/discharge (t_2)

1 Motivation

Contemporary expectations placed on the efficiency (thermal and economical) of Thermal Energy Storages (TES) and of interest in this work, where these storages are incorporating solar energy, are significantly influenced by the still relatively high price of such systems. Given the current high capture efficiencies of solar thermal collectors, attention needs now be turned to the effective transfer of the heat won, stored and utilised in the largely thermally indirect processes thereafter.

Until now many empirical studies on the heat transfer involving free convection (that resulting from temperature induced buoyancy) of varying geometrical instances and fluid/gas properties have been performed (see Appendix A). Problems arise when one chooses a setup of a deviating or complicated geometrical nature.

The powerful (and time consuming) non-intrusive methods of Particle Imaging Velocimetry and Laser Induced Fluorescence offers new opportunities in the observation of actual convective phenomenon. In how far these methods can assist in the experimental determination of heat exchange processes in TES tanks and whether resulting improvements in thermal and economic efficiencies can be achieved has not yet been examined closely.

2 Aim

The intention behind the work reported here is to investigate the capabilities of the Quantitative Flow Visualisation (QFV) techniques of Particle Imaging Velocimetry (PIV) and Laser Induced Fluorescence (LIF) in the observation of heat induced buoyant fluid convection within solar TES tanks and identify possible ways for the elucidation of *convective heat transfer* and mixing phenomenon in exemplary TES configurations.

Divided into two experimental parts typical operating conditions involving charging of a TES with an immersed helical coil heat exchanger and discharging a TES with an internal Domestic Hot Water (DHW) tank (Combitank) are investigated with calorimetric and PIV measurements. As will be discussed later in Section 4.1.2, the calorimetric measurements were intended to support information won from the combination of PIV and LIF vector and temperature field measurements. During the project however it was realised that the implied use of hazardous chemicals (up to 800 litres of toxic water would need disposed of from time to time), long calibration times and the limited stability (with time) of these calibrations implicit of the LIF method would be too time consuming to be included within this project time-frame. For this reason only calorimetric measurements were used to attain insight into temperatures on heat exchanger connections as well as over the TES's height.

3 Theory

In the case of a TES, factors leading to a reduction in storage efficiency result from the following physical limitations:

- heat given to the surrounding environment,
- heat conduction from hot to colder fluids in tank,
- heat conduction through the tank wall (often metal) and

- mixing (destruction of stratification) during charge/discharge periods.

A methodology that considers all of the above system efficiency losses is not known to date and more importantly, the synchronous consideration of tank losses and internal loss due to mixing remains primitive at best. In the case of the experimentation presented in this report, the same tank was used in all cases such that the losses to the environment were assumed to remain relatively constant between experiments and therefore considered negligible in this project.

To address the loss in energy quality occurring during charge and discharge sequences, the principle of entropy or more specifically the observation of when and where entropy is generated (unusable energy), is adapted to two experimental setups, the knowledge of which in combination with PIV observations may help to identify critical geometries or system parameters.

A typical supply-side immersed coil heat exchanger chosen on account of the relationship of the coil tube diameter to the pitch between helical coils is examined over varying charge mass flows and coil pitches. Subsequently two geometrically varying internal DHW combitanks configurations are examined for their efficiency in the supply of DHW for differing discharge volumes and mass flows (for literature and market research see [3]). In both instances the effect this charging or discharging has on the 'quality' of thermal energy within the store is evaluated based on the *principle of entropy generation.*

3.1 The Balancing of Entropy and Exergy in a Thermal Energy Storage

While a number of methodologies for investigating and comparing TES's exist (National and/or European Standards), most rely on the energy efficiency or ratio of energy recovered to that originally introduced as indication for effective operation. This perspective fails however to acknowledge certain qualities of a TES like how nearly the system reflects an ideal case, how stratified the storage is (affecting indirectly the solar collector performance; see [20, 2]) and the relationship of the temperatures of the supplied and recovered thermal energy to their surroundings.

Extension beyond the first law of thermodynamics to include the second introduces a property with which we are able to evaluate the capture and preservation of high temperature energy in stratification. This criterion states simply; high temperature heat can easily satisfy the needs of low temperature heat but not vice versa. This leads to a subdivision of any energy into that which we can use and that which we cannot. The ability of energy to do work which is useful is called *exergy* and the part which cannot be utilised is called *anergy*;

$$\begin{aligned} Energy &= Exergy + Anergy \\ E &= \Xi + A \end{aligned} \tag{1}$$

We begin by observing the boundaries of our system. Given the residual influence the tank insulation has on cyclical processes and vertical heat transfer, the system boundary is set inside from this. Furthermore, balancing the energy entering and exiting the tank requires accounting for the inlet and outlet used for charging and discharging sequences, be they directly or indirectly coupled to the TES system.

What we seek is a method for determining the generation of entropy ($S_{1\rightarrow 2_{irr}}$) in the form of mixing phenomenon. The complete entropy generation occurring between the

beginning t_1 and end t_2 of the test sequence is found using

$$S_2 - S_1 = S_{Q_{1\to2}} + S_{1\to2_{irr}} + \int_1^2 \dot{m}(s_{in} - s_{out})\mathrm{d}t \tag{2}$$

where the net heat transfer that occurs between states 1 and 2 is often expressed as

$$S_{Q_{1\to2}} = \int_1^2 \frac{\delta Q}{T(Q)}.$$

Analogously Equation 2 can be reorganised to determine the loss in exergy such that

$$\Xi_{1\to2_{loss}} = \Xi_{tes_1} - \Xi_{tes_2} + \Xi_{Q_{1\to2}} + \int_1^2 \dot{m}(\xi_{in} - \xi_{out})\mathrm{d}t, \tag{3}$$

where the method from Appendix D serves for the calculation of exergy (Ξ_{tes}) in the TES at a given state.

The question regarding the reference temperature T_0 against which the quality of the energy in the exergy calculations is compared is theoretically dependent. Often the cold water inlet temperature is chosen as it is the lowest temperature in the system. If one seeks semblance with the EN12977-3 norm for testing Combisystems, one would choose the ambient temperature of $20°C$ and condition the inlet temperature as such. Rosengarten [15] showed that it is also possible the think of the temperature at which one consumes the energy as the reference point for any TES and, calling it a temperature of *delivery*, set it at $40°C$. To simplify the matter, the cold water inlet temperature of $10°C$ shall be used for the following exergetic evaluations.

For evaluating the sequences together a so called stratification efficiency over the interval {0;1} is used to relate the different test sequences to one another. Huhn [5] developed a dimensionless value embodying the point the TES finds itself between an ideal charge or discharge of the TES and the worst-case scenario in which no stratification occurs ('fully-mixed store') with

$$\begin{aligned}\zeta &= 1 - \frac{S_{irr_{real}}}{S_{irr_{mix}}} \\ &= 1 - \frac{\triangle\Xi_{real}}{\triangle\Xi_{mix}}.\end{aligned} \tag{4}$$

Any real TES temperature profile will show some degree of thermal stratification but, as this stratification efficiency purports to measure the real case against some 'ideal' stratification, the realisation that this 'ideal' case is physically unattainable (imagine an infinitely thin film at the very top horizontal cross section of the TES having an almost infinite temperature) makes the seemingly small values less insignificant.

4 Method

For the sake of optical access for PIV and LIF measurements a specially fabricated glass tank measuring $80 \times 80 \times 180cm$ was insulated on all sides with 7cm of insulating foam. Windows were cut into the foam that could be removed during experiments in moments when PIV recordings were made.

A temperature recording function was programmed in LabView for the acquisition of calorimetric data during experiments at a frequency of $1Hz$. Thermo-sensors are of type Pt100 (Platinum resistive thermometer 100Ω) and were calibrated with linear correction in a thermostat bath over the interval $(10, 30, 50, 70, 90, 110)°C$ which achieved a confidence envelope of $\pm 0.05K$. One problem associated with Pt100 thermometers is their latent reaction to oscillations and quick fluctuations in measured fluid temperature resulting from the heat capacitance of the probe. This can lead to a temperature disparity between the actual dynamic temperature and that which is recorded as big as 5% of any jump between two sequential readings. On the assumption that no temperature change in the system greater than $1°/sec$ is expected, our envelope of uncertainty expands to $\pm 0.1K$ for any given reading. A dialogue showing the recording nodes in LabView is shown in Figure 1.

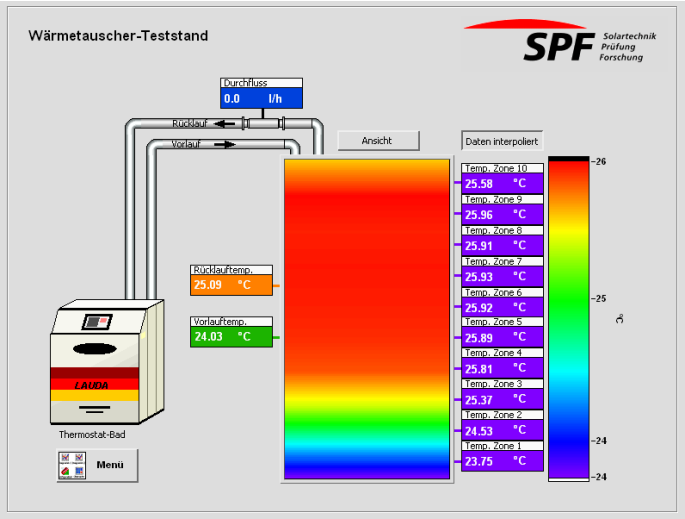

Figure 1: Overview of the Laboratory setup showing calorimetric measurement points. The *Vorlauf* and *Rücklauf* measuring nodes are interchangeable between experiments involving charging through the immersed coil heat exchanger (in which the Lauda Thermostat bath is connected) or discharging via an internal DHW tank (where normal tap water is connected). Both are regarded exergetically as hx

4.1 Quantitative Flow Visualisation (QFV)

For a general introduction to the QFV techniques considered in this project refer to Appendix B.

The integration of QFV into any laboratory is a time consuming challenge. Not only are the techniques in themselves abstract in nature but applying any one of them to the problem in hand requires the consideration of many limiting factors that one can only learn in the process. Take for example the bending and or stretching of an image plane from water travelling out through glass into air orientated at an angle to both camera acquisition and image plane. Although there are calibration techniques to account for this, given a limited time frame one must accept certain limits to the detail one can acquire to get the job done. Often during this project problems involving the water quality, particle density,

laser sheet generation or any number of other small hindrances added to the project time, at times doubling that which was estimated and planned for.

This does not however detract from the powerful non-intrusive nature of the results one can obtain given enough time to do so. Apart from any modifications one must make to the object of interrogation (e.g. optical access), the detail and accuracy of observed phenomenon in situ opens up a huge potential for correlation to the theoretical and numerical (Computational Fluid Dynamics) methods seemingly so far from being validated in certain areas, of which free convection is one.

4.1.1 Particle Imaging Velocimetry (PIV)

The PIV system utilised in this project compromising of a $125mJ$ double pulsed NdYAG, two CCD (charged coupled device) cameras, a triggering computer and a one-dimensional translation (1800mm) system was installed for *2D* planar PIV (see Appendix B.1 for details) acquisition of images between $10cm \times 10cm$ and $30cm \times 30cm$ with the capacity to translate vertically between the top and bottom of the glass tank. Computational software allows the *stitching* of obtained vector fields together with the limitation on these acquisitions being that there is always an implied time delay between any two images lying side-by-side. Although interpolation over any overlapping areas is implemented, it is often recognisable where vector fields have been stitched together. What one hopes to visualise

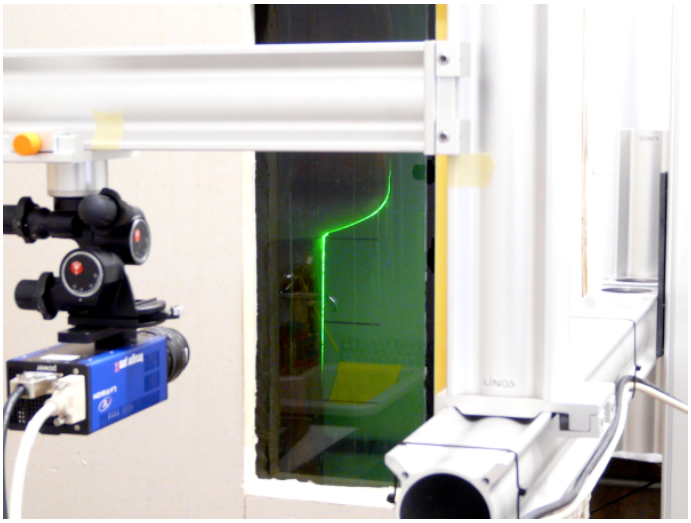

Figure 2: Picture taken during a PIV recording showing the setup of the system acquisition

and quantify is the mass transport in and around the geometrical bodies experiencing free convective heat transfer, such that not only is a better understanding of boundary layer phenomenon made possible, one can also extract kinetic energies across predefined boundaries in the system for looking into mixing energies and their influence on entropy generation. Although such possibilities were discussed, the time required to undertake such studies responsible was well beyond the scope of this project.

During any experiment undertaken, a series of PIV scans along one optically accessible side of the tank were performed repeatedly at predefined points within the experiment.

4.1.2 Laser Induced Fluorescence (LIF)

As mentioned in Section 2, no LIF measurements were performed for the experiments undertaken. An understanding into the requirements for integrating LIF showed that it was indeed overzealous to believe it was possible in the short time available.

When considering a large experimental object containing a cubic metre of water, considerable time is required to heat the fluorophore containing water to predefined homogeneous temperature points for calibration of the image acquisition to the intensity of fluorophore emission; at times more than the experiment itself. It is understood that such calibrations are then only valid for one or two days at most, as so called *photo-bleaching* (see Appendix C) occurring from the laser pumping make re-calibration necessary by then.

Given ample time however, this method promises an application to the quantification of free convective heat transfer in that the acquisition of temperature fields in the proximity of heat transfer surfaces (in boundary layers) could make direct integration across the temperature gradients for the local clarification of convective heat transfer coefficients (Nusselt numbers) possible.

4.2 Indirect Charging of a TES with an Immersed Coil Heat Exchanger

It is well understood that the distance an immersed coil heat exchanger (IHX) has between coils (*pitch* of coil growth) plays a significant role in the heat transfer coefficient [8]. The closer these coils are orientated in the vertical axis, the hotter and stronger the convective flows are that flow from one coil up onto the next. Although a greater velocity in convection can be synchronously expected, this increase in boundary layer velocity does not influence the heat transfer numbers as much as the temperature difference between heat exchanger and that part of the storage medium caught in the boundary layer.

For purposes of confirming this knowledge in lieu of improved observation through PIV and for conditions found in typical solar thermal applications, an IHX was installed and the convective boundary forces were observed over a variety of heat exchanger volume flow rates ($60, 100$ and $150 l/h$) representative for an exchanger of this size utilised in predominately *medium to high flow* systems. In each case the distance between coil turns in relation to the tube diameter, the so called *pitch-to-diameter* p/D ratio, was varied over values found most commonly within current TES designs (see market research [3]); namely between 0.3 and 1.

The investigated IHX (shown in Figure 3) has a tube diameter of 32mm and a distance between the centre of one tube to the next of 44mm which placed in context means that $p/D = \frac{44-32}{32} = 0.375$. This was subsequently stretched out to achieve p/D of 0.7 and 1.0 by way of wooden templates. To examine simply the effect p/D has on the performance of an IHX, the following calculations were performed over the relatively short charging times for each experiment.

Typically an IHX installed as in Figure 3b receives the hot water to the inlet at the top of the IHX, with the cold outlet exiting at the bottom. In this sense should any thermal stratification take place in the range of TES in which the IHX finds itself, a pseudo cross-flow heat exchange can be observed.

The energy the heat exchanger delivers is defined through the relationship

$$\dot{Q} = \dot{m} c (T_{hx_{in}} - T_{hx_{out}}). \tag{5}$$

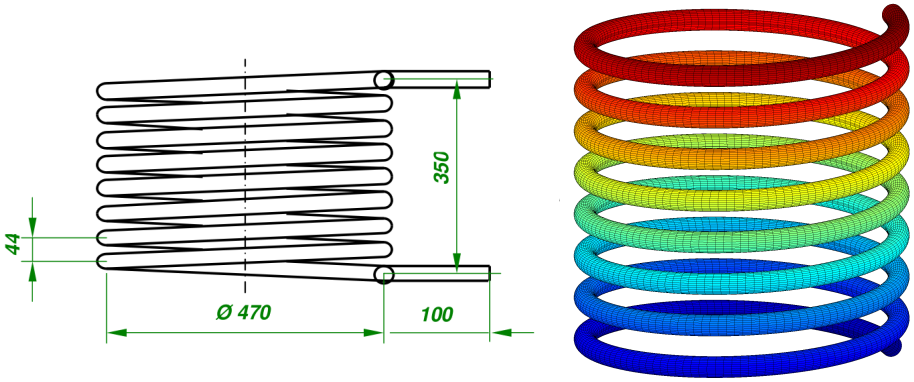

(a) Dimensions of IHX where $p/D = 0.375$

(b) 3D visualisation of IHX where $p/D = 1.0$

Figure 3: Investigated *off the shelf* immersed coil heat exchanger

In each charging run the heat transfer rate $\dot{Q}$ was held at a constant $3kW$ by attenuating the thermostat bath outlet temperature based on a Pt100 sensor on the heat exchanger return fluid to maintain a constant difference between inlet and outlet temperature. This coincides to what one might expect from 4 to $6m^2$ of solar collector in good solar conditions.

On the assumption there is a homogeneous storage temperature surrounding the IHX [1] one can use the log mean temperature difference;

$$\Theta_m = \frac{(T_{hx_{in}} - T_{hx_{out}})}{\ln\left[\frac{T_{hx_{in}} - T_{tes}}{T_{hx_{out}} - T_{tes}}\right]} \tag{6}$$

to approximate the overall heat transfer coefficients with and without consideration for the heat exchanger surface area by Equations 7 and 8 respectively.

$$UA = \frac{\dot{q}}{\Theta_m} \tag{7}$$

$$\overline{h_o} = \frac{\dot{q}}{(A)(\Theta_m)} \tag{8}$$

The so called Nusselt number which describes a medium independent measure of the relationship from convective to conductive heat transfer within the boundary layer is expressed with

$$\overline{Nu} = \overline{h_o}\frac{d}{\lambda_{h_2o}}. \tag{9}$$

The results from the experiments are found in Section 5.1.

[1] This is an assumption leading to error in the case of high thermal stratification

4.3 Indirect Discharging of a TES combining domestic hot water and heating

As time constraint inhibited the detailed selection and testing of many combitank variations, two tanks were taken from those considered as having significantly different geometries but similar functioning principals.

The method of discharging by way of a combitank is made somewhat complicated in that time plays a significant role in the heat transfer process on account of the large volume unit to heat exchanger area. The measurements were developed on a principle of repetition in that each tank was discharged of a given fractional volume from the total volume V_{dhw} of the internal domestic hot water tank ($0.3, 0.6$ and $1 \times V_{dhw}$) at two differing volume flows ($\dot{v} = 240$ and $600 l/h$) in sequences where waiting times between discharges of up to one hour were allowed. The discharging was repeated until either the TES mean temperature dropped below $45°$ or 4 repeated discharges were reached. Through repetition of V_{dhw} fraction and $\dot{v}$ variants one expects to manifest characteristics in the tanks exergetic performance adhering to the symbolic consumer habits of small, medium and large consuming households. Results of the indirect discharge experiments are found in Section 5.2.

Figures showing the installation of the two tanks where details and the laboratory setup are visible are given in Figures 4a and 4b for the so called *Horseshoe-nail* DHW tank and in Figures 4c and 4d for the immersed heat exchanger integrated DHW tank.

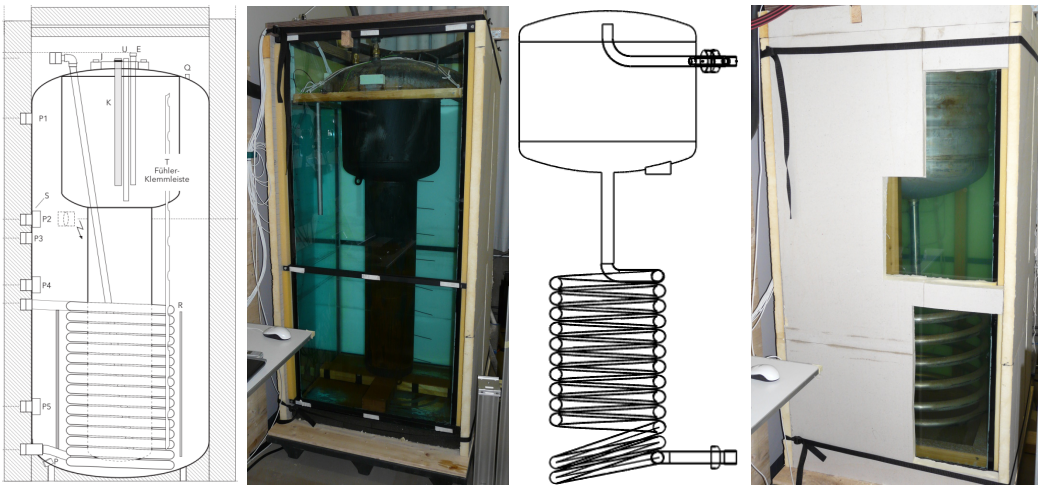

(a) *Horseshoe-nail* **(b)** $V_{dhw} = 163l$ **(c)** IHX integrated **(d)** $V_{dhw} = 230l$

Figure 4: Combitank DHW installations

Before the begin of a discharge sequence, the TES was conditioned as near as possible to a homogeneous temperature of $60°C$. The precondition that this creates is that we are starting the discharge sequences from a fully charged tank which, relating back to Section 3.1, is considered as the *worst case* state one can find the tank in. What we mean by this is that the tank is fully charged but is in a fully mixed state, meaning that in attaining such a state, already the highest amount of mixing entropy has been generated in getting there. From this point further entropy is generated but stratification of any form, as one would expect in real cases, improves the relativity of stored exergy to stored

energy. However, in addition to this and of opposite influence for this relationship, there exist no *Thermoclines* (steep gradients in temperature) which would - if present - retard mixing to a degree.

5 Results and Discussion

Exemplary analysis of the accumulated data are collected together here for evaluation.

5.1 Charging of TES with an IHX

Evaluation of the results tend towards agreement with previous work (see [8]) in that the relationship of convective to conductive heat transfer as expressed in the Nusselt number increase in relationship to an increase in p/D. One must observe these results with caution though as the erroneous nature of the intended *constant* power ($\dot{Q}$) is evident upon closer inspection of the third column in Table 1 and this error is carried through in the performance calculations made thereafter. Of additional concern is the uncertainty associated with using temperature measurements from Pt100 thermo-sensors instead of the less discrete and indeed better instantaneous method of measuring tank temperature with LIF.

Parameters		Calculations			
p/D	$\dot{m}$ $[l/h]$	$\dot{q}$ $[W]$	UA $[W/K]$	Nu $[-]$	h_o $[W/m^2.K]$
0.3	60	3049	467	2.1	389
0.3	100	2897	224	1.01	187
0.3	150	2833	222	1	185
0.7	60	2732	450	2.03	375
0.7	100	2943	226	1.02	189
0.7	150	3017	233	1.05	194
1.0	60	3045	511	2.3	426
1.0	100	2999	243	1.1	202
1.0	150	3105	245	1.1	204

Table 1: Results for charging the TES with the immersed coil heat exchanger. Calculations were performed over a period of 5000 seconds of stable charging results of which averages are shown.

The effect flow rate has on the Nusselt number is worth noting in that the apparent importance convective heat transfer plays for $60l/h$ when compared to the other two flow rates for all experiments can be explained through the higher temperature difference required to attain the same power and the stronger buoyancy associated with this.

On inspection of the TES performance for each of the IHX experiments given in Table 2 we can observe two apparent trends one might like to associate with the insights gained on Nusselt numbers from Table 1. Not only is there a tendency for a higher ratio of exergy input to exergy losses generated (viewed in the second last column) but we are also seeing an obvious increase in the stratification efficiency as one increases the p/D relationship (last column).

Parameters		Exergy Balance				Performance	
p/D	$\dot{m}$ $[l/h]$	Ξ_L $[MJ]$	Ξ_{tes_1} $[MJ]$	Ξ_{tes_2} $[MJ]$	Ξ_{hx} $[MJ]$	Ξ_{hx}/Ξ_L $[MJ]$	ζ $[-]$
0.3	60	0.903	0.0186	0.467	1.35	1.5	0.0556
0.3	100	0.664	0.0172	0.454	1.1	1.66	0.0456
0.3	150	0.557	0.0159	0.425	0.966	1.74	0.0277
0.7	60	0.93	0.0372	0.744	1.64	1.76	0.117
0.7	100	0.744	0.0211	0.657	1.38	1.85	0.0989
0.7	150	0.711	0.0188	0.722	1.41	1.99	0.0937
1.0	60	1.04	0.0134	0.827	1.85	1.78	0.158
1.0	100	0.811	0.0204	0.734	1.52	1.88	0.118
1.0	150	0.842	0.0245	1.01	1.83	2.17	0.111

Table 2: Results of the exergetic balance for charging the TES with the immersed coil heat exchanger

Chosen for their indication of recurring phenomenon, PIV recordings of the two extreme p/D cases have been included to help diagnose the results found in Tables 1 and 2. Each recording is the averaged derivation from thirty recordings taken at the rate of approximately $8Hz$; ultimately we are seeing around four seconds of mean fluid flow. This offers the benefit of removing minor local phenomenon like vortices and turbulence in the favour of average mass transfer information. In Figure 5 we can see how the plane of observation relates to the coils of the IHX, shown as streamlines traced on the PIV vector map.

What is evident upon comparing Figure 6 with 8 and 7 with 9 is firstly the different overall height of the IHX within the tank, influencing the volume of storage fluid in which the same delivery power can be dispersed. The strong buoyant plume erupting from above the IHX in for $p/D = 0.3$ (Figure 7) - which seems to gather strength inside the IHX coil - is the reason for the greater mixing numbers we are seeing within Table 2 for low p/D. In comparison to this we can see that this same cumulative kinetic movement seems to be significantly discouraged between coil turns in the case of $p/D = 1.0$ seen in Figures 8 and 9, resulting in a much smaller plume and therefor less global mixing.

As already mentioned, without information on the temperatures around the IHX coils (LIF) it is not possible to comment in any detail on the local Nusselt numbers within the boundary layers visible in all PIV recordings, however interesting such study might prove. Extended investigation could lead to interesting findings resulting in possible recommendations to manufacturers in how they might improve the design of IHX's; to increase the specific heat transfer and thus the economic effectiveness of them. This is especially true when considering the increase in variety of IHX's used in contemporary solar thermal storages in ever varying methods of charging from heat sources and discharging from heat sinks.

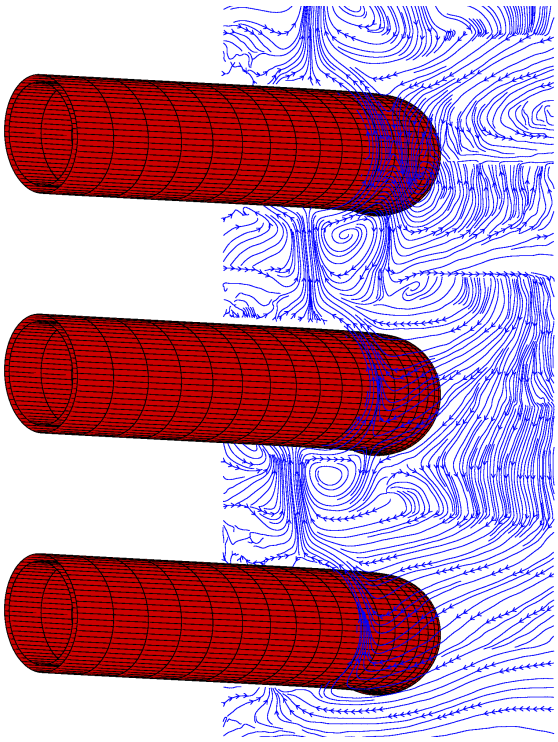

Figure 5: Graphic from a selected experimental PIV recording showing the orientation of the IHX to the recording plane; shown here as streamlines calculated over the vector field.

5.2 Discharging of Combitank DHW

On comparing the tables for the two Combitank DHW configurations we see marginal difference in the ratio of exergy discharged to exergy lost in favour of the IHX integrated combitank, calculated in the second last column of both Tables 3 and 4, which however does not allow definite inference of configuration performance due to inconsistencies in experiments such as the varying TES states between t_1 and t_2, different extracted exergies and the difficulty in preconditioning consistently.

Parameters		Exergy Balance				Performance	
V_{dhw} fraction	$\dot{m}$ $[l/h]$	Ξ_L $[MJ]$	Ξ_{tes_1} $[MJ]$	Ξ_{tes_2} $[MJ]$	Ξ_{hx} $[MJ]$	Ξ_{hx}/Ξ_L $[MJ]$	ζ $[-]$
0.3	240	4.49	19.6	11.1	-4.02	0.895	0.0455
0.3	600	4.71	19.4	10.8	-3.94	0.837	0.0254
0.6	240	4.8	19.6	8.78	-6.02	1.25	0.0279
0.6	600	7.11	23.2	8.14	-7.94	1.12	0.00463
1.0	240	5.73	18.9	7.05	-6.1	1.06	0.0155
1.0	600	5.85	18.9	7.58	-5.46	0.933	0.00178

Table 3: Results of the exergetic evaluation for discharging the TES with a horseshoe-nail combitank configuration

Although we are dealing with very small stratification efficiencies, it can be seen that

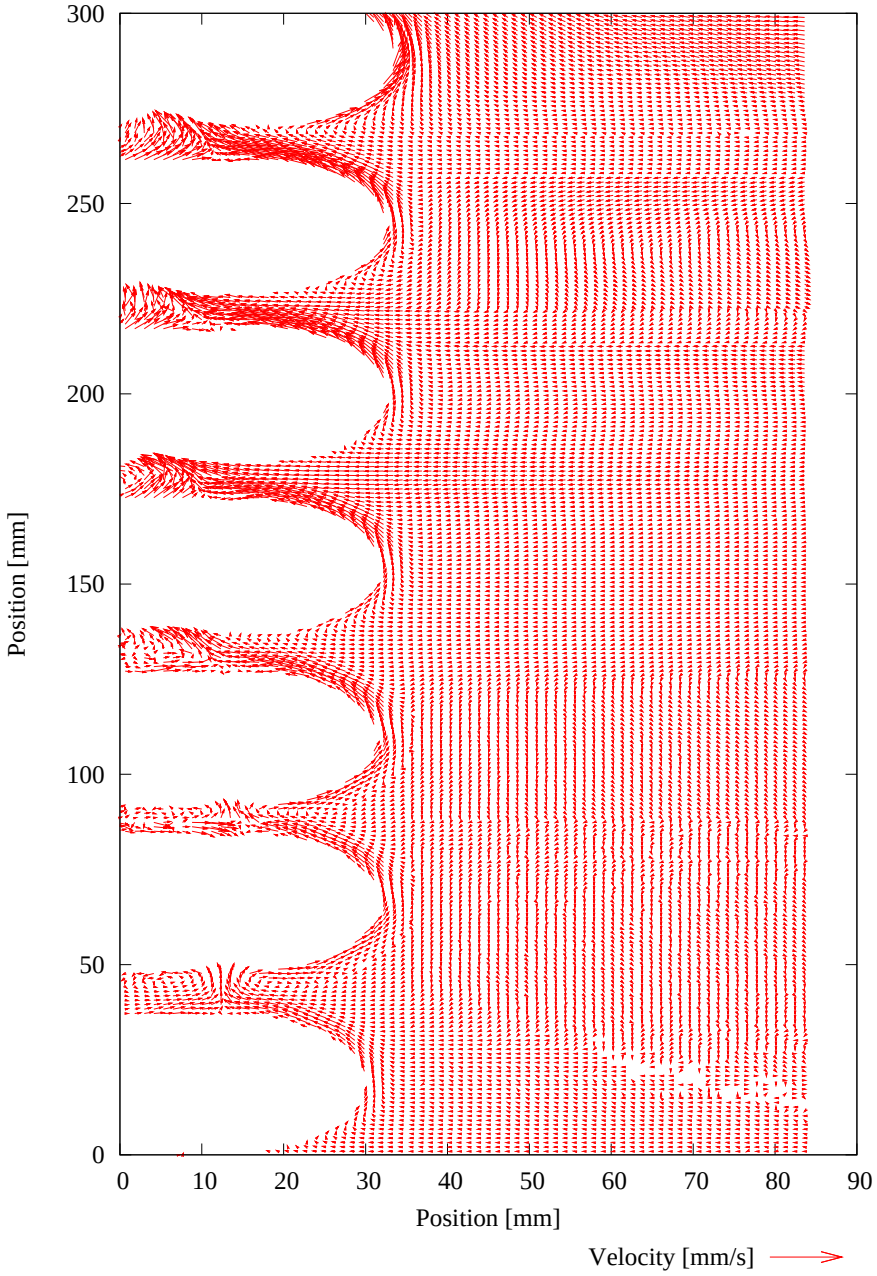

Figure 6: Lower PIV Recording showing the immersed heat exchanger with a $p/D = 0.3$ and a volume flow of $150 l/h$.

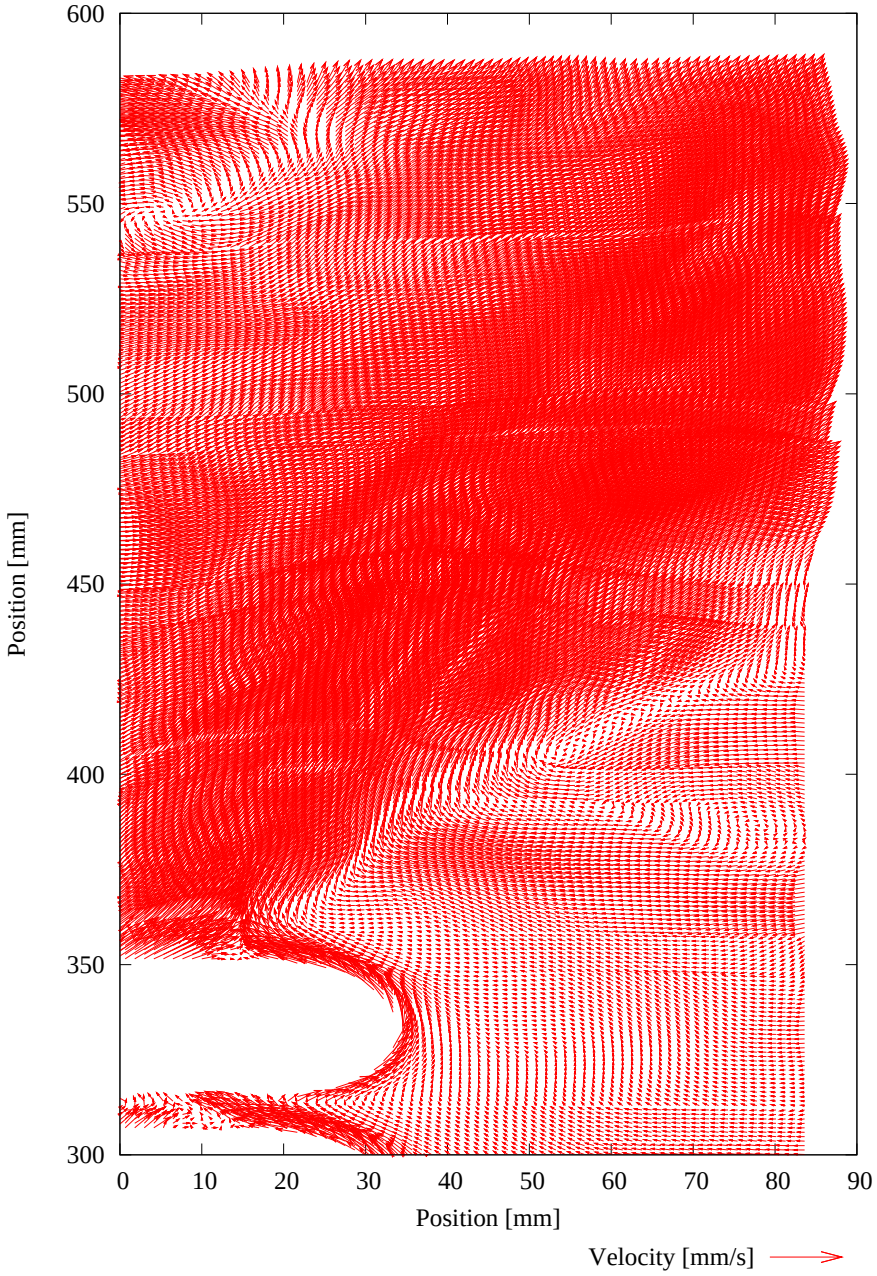

Figure 7: Upper PIV Recording showing the immersed heat exchanger with a $p/D = 0.3$ and a volume flow of $150l/h$.

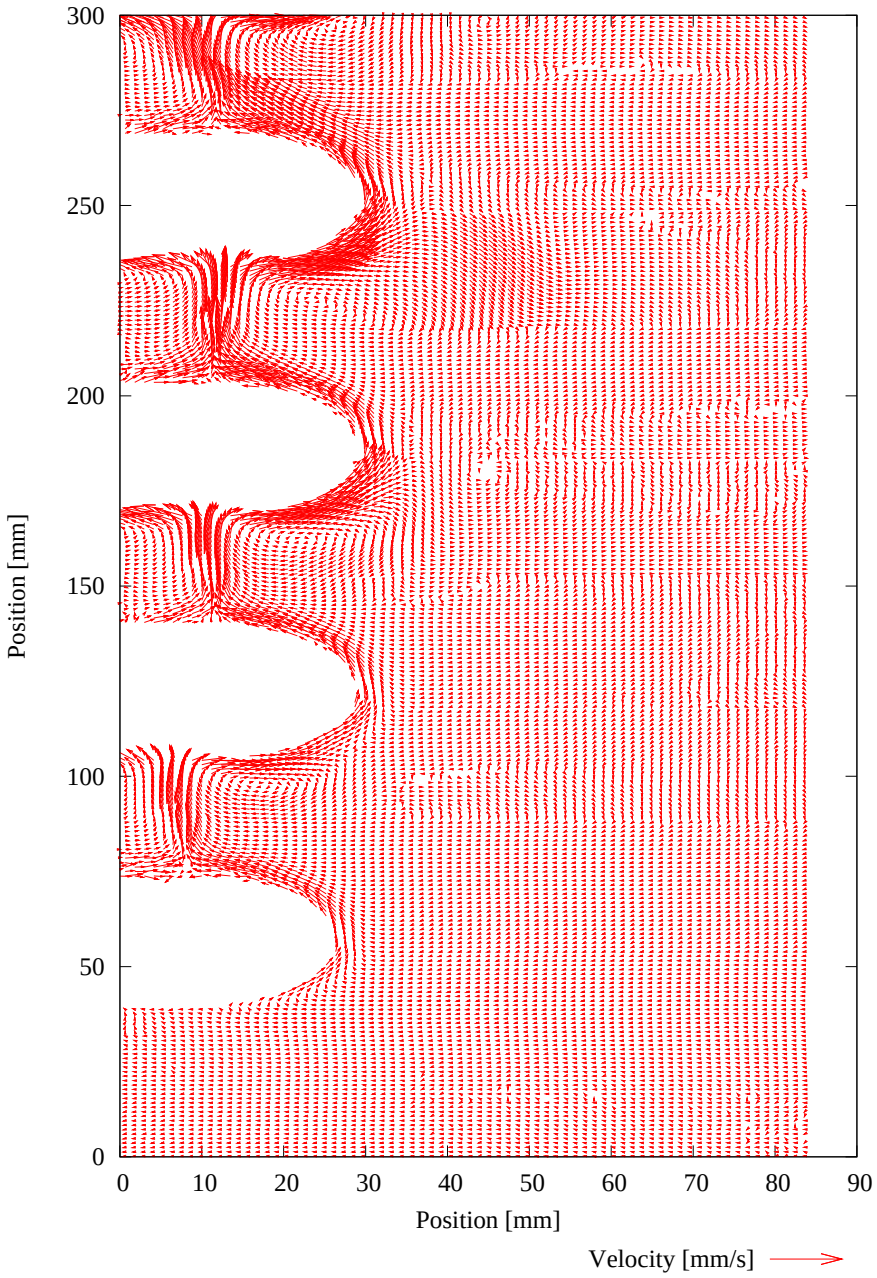

Figure 8: Lower PIV Recording showing the immersed heat exchanger with a $p/D = 1.0$ and a volume flow of $150 l/h$.

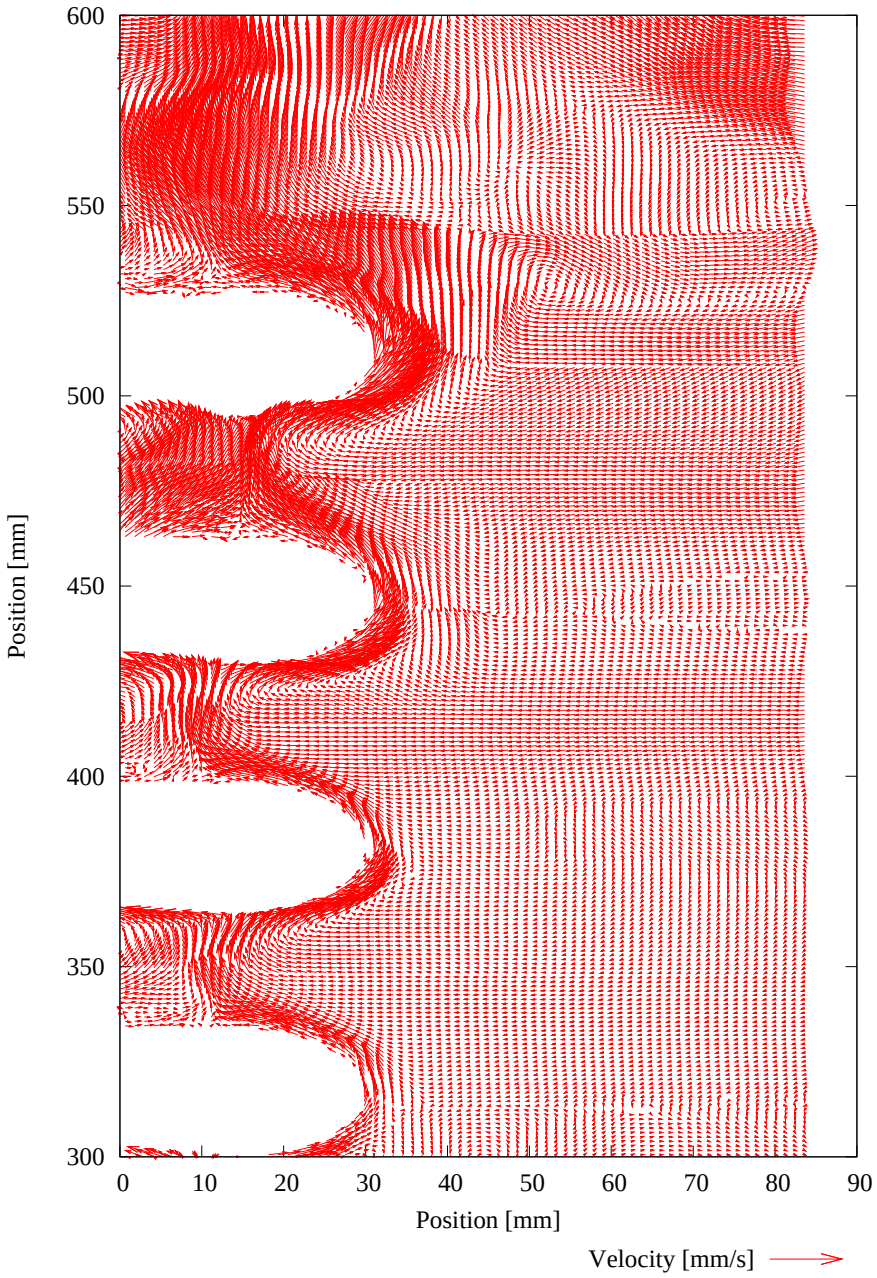

Figure 9: Upper PIV Recording showing the immersed heat exchanger with a $p/D = 1.0$ and a volume flow of $150 l/h$.

Parameters		Exergy Balance				Performance	
V_{dhw} fraction	$\dot{m}$ $[l/h]$	Ξ_L $[MJ]$	Ξ_{tes_1} $[MJ]$	Ξ_{tes_2} $[MJ]$	Ξ_{hx} $[MJ]$	Ξ_{hx}/Ξ_L $[MJ]$	ζ $[-]$
0.3	240	2.61	20.6	14.4	-3.57	1.37	0.0981
0.3	600	5.92	24.3	12.8	-5.54	0.936	0.0194
0.6	240	4.12	21.5	8.49	-8.87	2.15	0.00649
0.6	600	5.51	19.9	6.61	-7.77	1.41	0.0162
1.0	240	5.05	19	5.6	-8.31	1.65	0.0495
1.0	600	6.53	22.6	6.83	-9.23	1.41	0.0187

Table 4: Results of the exergetic evaluation of discharging the TES with the immersed coil heat exchanger combitank configuration

for each experiment the higher flow rate generates significantly more entropy. There is a tendency for higher stratification efficiencies for the IHX integrated combitank, a matter confirmed by the exemplary temperature profiles in Figure 10, however whether one can draw as such conclusions of its better performance is hard to say in light of the errors already mentioned. Evaluation of the suspicions implied from the calorific measurements

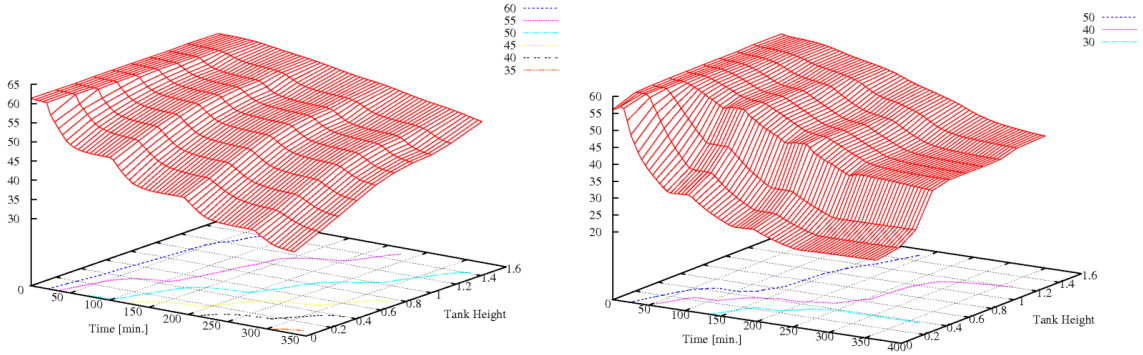

(a) Horseshoe-nail combitank **(b)** IHX integrated combitank

Figure 10: Meshes of experimental temperature matrix for $V_{dhw} = 1.0$ and $\dot{v} = 240l/h$ showing the differing profile development throughout the evaluated experimental range.

is offered in the PIV recordings visible in Figures 11 to 14.

In the case of the horseshoe-nail geometry (Figures 11 and 12) it can be seen that an unbroken boundary layer is permitted travel without hindrance from where the neck begins (below the auxiliary heated volume at position $1100mm$ in Figure 12) to the bottom of the tank where the immersed coil heat exchanger solar supply would charge. This leads to a larger mixing over a greater height within the TES following discharge sequences in which sizable quantities of hot water are drawn.

What appears to occur within the IHX integrated combitank (Figures 13 and 14) is a disruption of surface boundary layer when observed over the total height of the TES. With this the vertical mixing of stratified layers is reduced which allows extraction of the heat from the bottom upwards, an observation confirmed by the temperature profiles over the tank heights for corresponding test sequences from each configuration.

As with IHX's, further investigation involving the method of LIF would lead to improved evaluation of stratification and mixing phenomenon for the benefit of design yet in contrast to the experimentation required for IHX, combitank systems are significantly more varying and require much effort to install and test in the PIV/LIF environment.

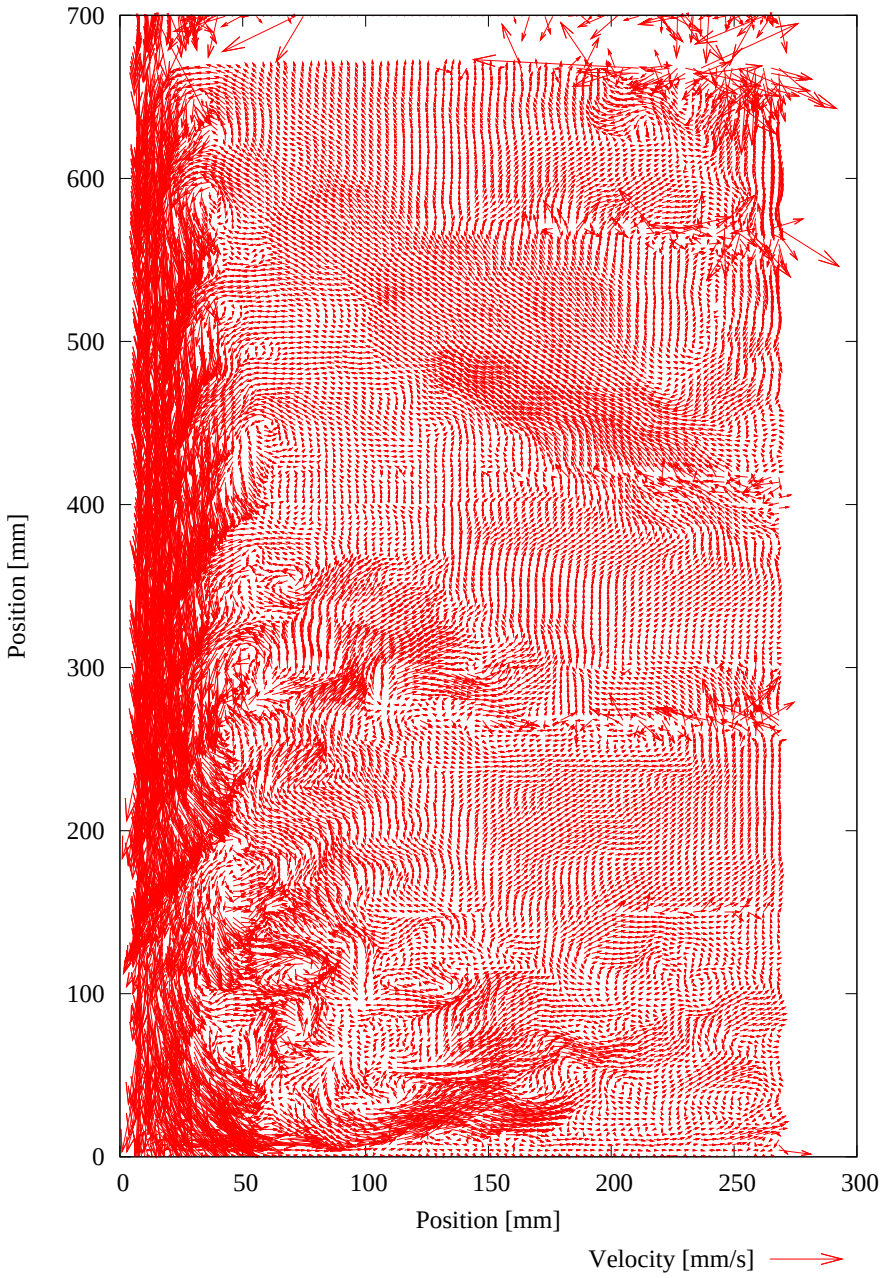

Figure 11: Lower PIV Recording showing bottom of horseshoe-nail combitank configuration following a discharge of $0.6 \times V_{dhw}$ at $600 l/h$.

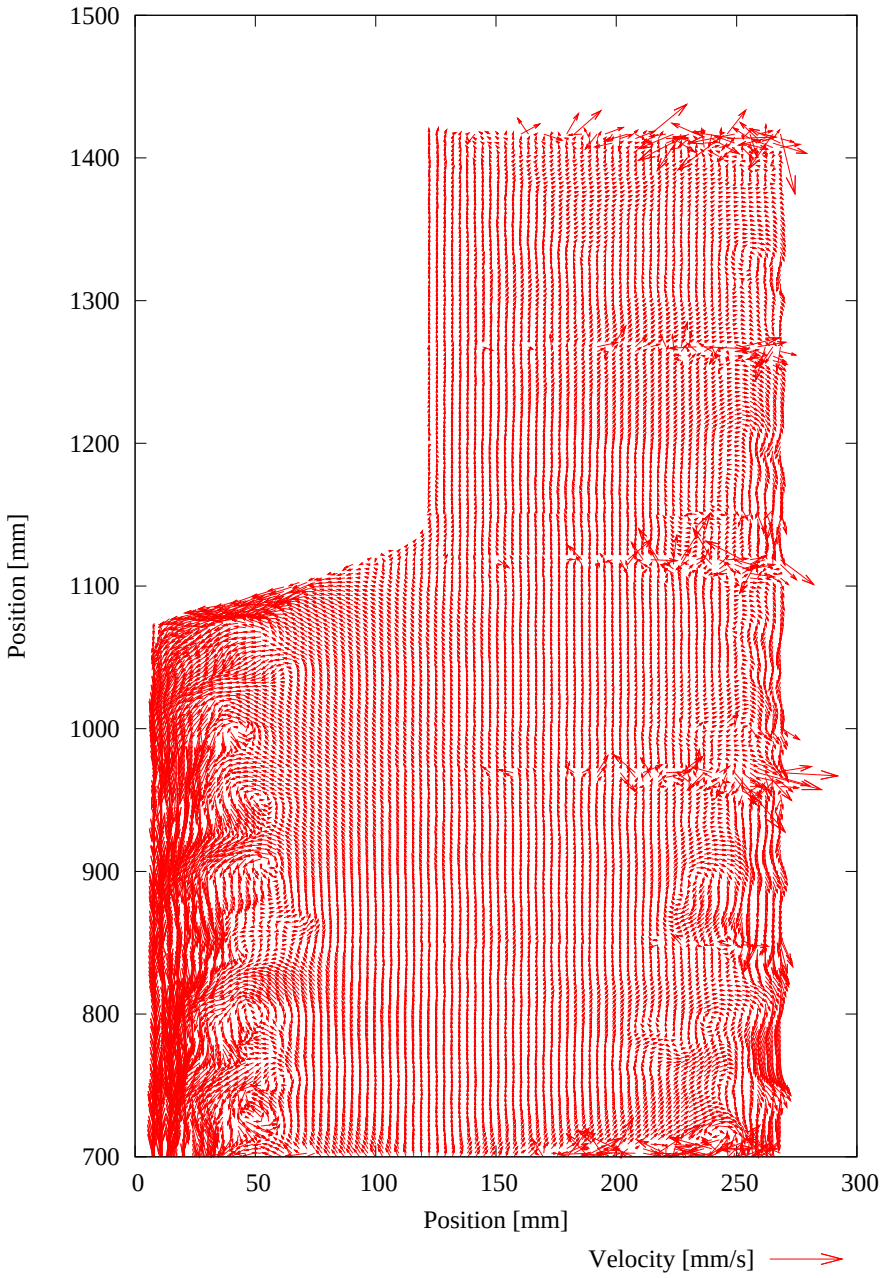

Figure 12: Upper PIV Recording showing top of horseshoe-nail combitank configuration following a discharge of $0.6 \times V_{dhw}$ at $600l/h$.

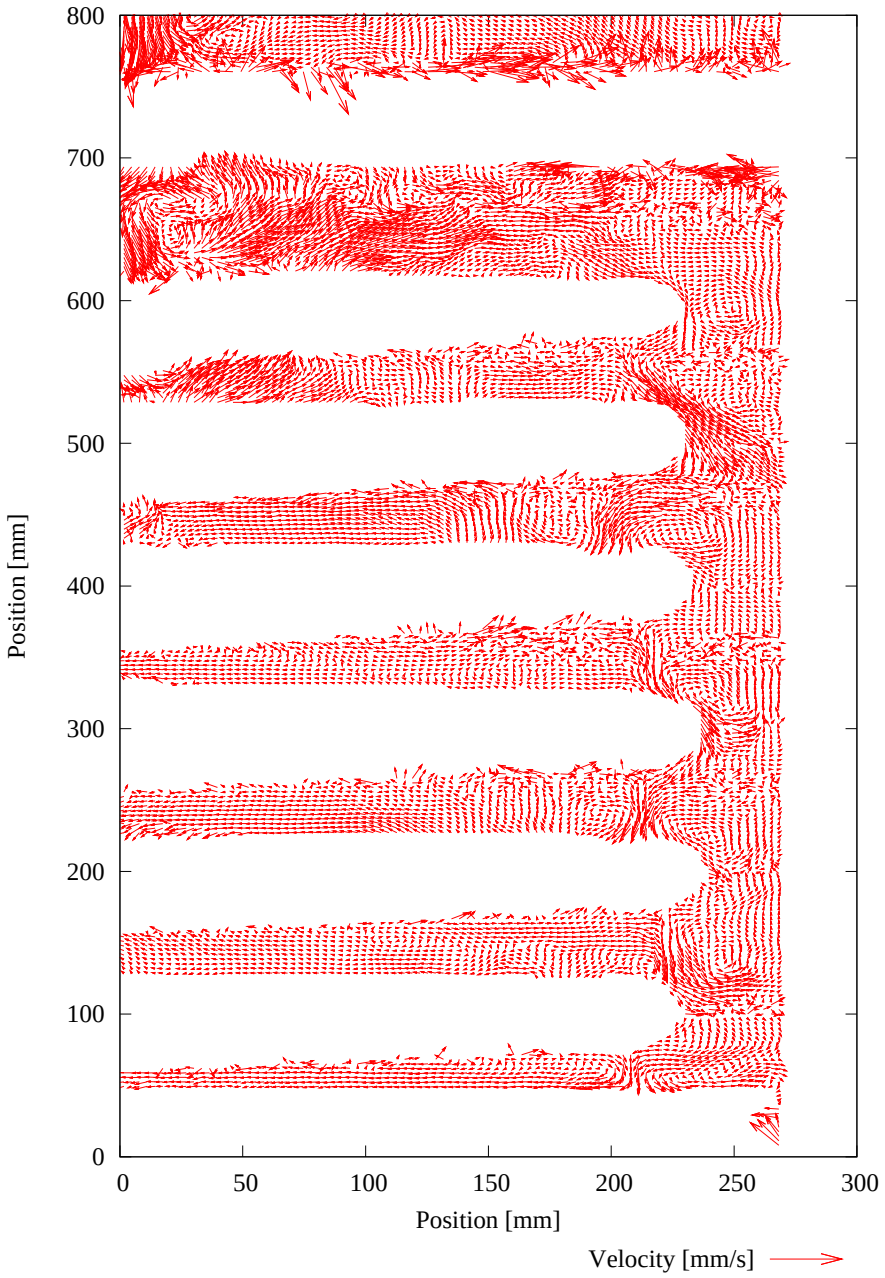

Figure 13: Lower PIV Recording showing bottom of immersed heat exchanger integrated combitank configuration following a discharge of $0.6 \times V_{dhw}$ at $600l/h$.

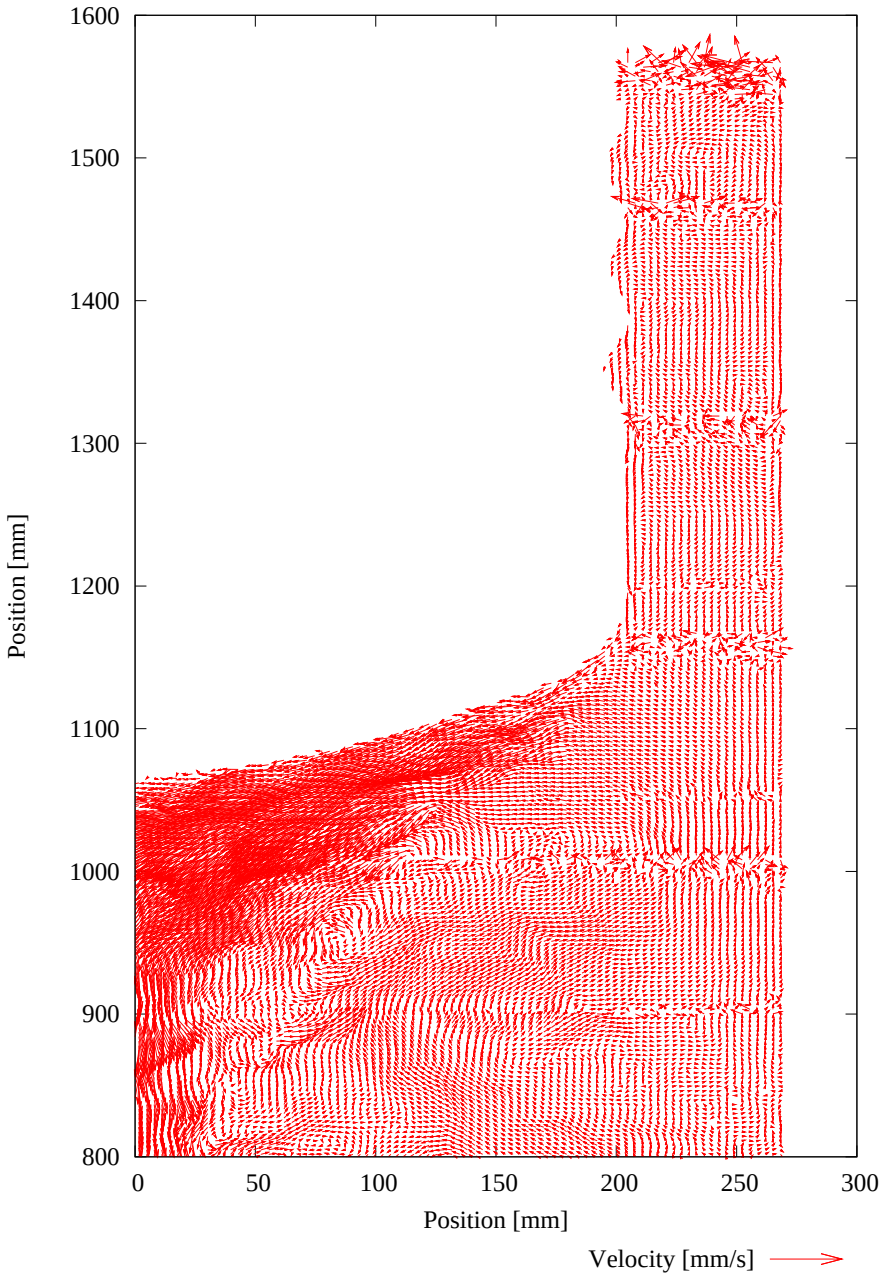

Figure 14: Upper PIV Recording showing top of immersed heat exchanger integrated combitank configuration following a discharge of $0.6 \times V_{dhw}$ at $600l/h$.

6 Conclusion and Outlook

Based on findings within the literature and resulting from the experimentation described in this report, the importance of efficiencies within Solar Thermal Energy Storages and the need for more work in this field has been realised.

While much is being invested into improvements of TES efficiencies through the implementation of various stratification ideas, many systems available on the market today make little to no account for improving immersed coil heat exchanger efficiencies through optimum p/D design nor the preservation of exergy in the form of stratification.

In this work it has been confirmed that the p/D relationship for any immersed coil heat exchanger has a significant influence on the heat exchanger coefficient, namely that an increase in heat exchange and an decrease in mixing phenomenon can be expected proportional to larger p/D ratios. In how far this relationship could effect the future design of immersed coil heat exchangers should be answered in further investigation.

On account of the experimentation on combitank domestic hot water configurations it can be seen that free convective heat transfer plays a significant role in the exergetic performance of a thermal energy storage.

In parallel to the experience gained in the evaluation of thermal energy storages in light of the second law of thermodynamics, much experience and competence has been gained in the measuring of convective heat transfer buoyant flows with particle imaging velocimetry; in particular the limitations to experimental execution have been explored in detail.

With the completion of this exploratory project one is able to make some recommendations for further work based on the knowledge gained in the complex experimental method as well as data analysis and handling including the preprocessing and post-processing of optical data. Further investigations should include:

- The exploration of Nusselt number (Nu_o) prediction models
- Annual TRNSYS simulations to look into the nature of tank performance, in particular to look at how often certain conditions within the tank occur. With such information one might improve the laboratory conditions and testing protocols used to evaluate stratification efficiencies.
- LIF measurements for the determination of local temperature boundary layers and Nusselt numbers through the integration of such boundary layers and in the studying of temperature distributions in questions of stratification efficiency.
- Detailed studies on immersed heat exchanger geometries where the varying surface areas, coil winds and p/D are explored under the associated manufacturing costs to determine where maximum performance with minimum additional costs may lie.

APPENDIX

A Background

The recent increase in the utilisation of thermal energy from renewable resources and the attempt to improve system efficiencies in the capturing and storage of it has drawn research and development efforts back to some of the fundamental problems first posed over one hundred years ago with Ludwig Prandtl's identification of boundary layer phenomenon. His ideas draw attention to the understanding of Thermal Energy Storages (TES) where the combination of thermal energy sources, storages and sinks require the implementation of heat exchangers through which the process of charging and discharging the TES can occur *indirectly*. Reference can be made on the one side to the frequent charging of TESs by way of an immersed coil heat exchanger or the discharging of TESs through an internal installed domestic hot water tank.

Taking a dynamic similitude approach to the practical application that his ideas had on the knowledge of boundary layer heat transfer, a number of attempts have since been made to contain the problem with approximations or empirical data for various flat plate, spherical and extruded cylindrical surfaces (e.g. [9, 13]).

More recently efforts have concentrated on correlating these empirical relationships to more complicated geometries found in real TES situations where heat transfer from *immersed helical tubes;* see [2, 11, 1, 21, 6, 8, 12], *horizontal tubes;* see [18, 19] and *mantle tanks;* see [17, 10] are considered. These studies compare prediction models embodying varying degrees of complication or computational fluid dynamics (CFD) with laboratory experimentation in the determination of *convective heat transfer coefficients* (embodied in the *Nusselt number*) and correlate these in part to characteristic geometric dimensions (e.g. surface lengths, heights and diameters) or fluid properties. There is no known methodology within the literature for calculating the convective heat transfer of a given integrated (immersed) heat exchanger.

Immersed coil heat exchangers are widely implemented due to their compact geometry and large surface area per unit volume. The newly emerging tank-in-tank DHW geometries have a contrary surface area to unit volume relationship, which leads to relatively low heat transfer power, longer stability times and smaller convective forces.

B Imaging Velocimetry

Over the years a number of *single-point* methods (such as hot-wire probes or laser doppler anemometers LDA) have been developed which can determine the local velocity vector with its three components and with very good temporal resolution (kHz). Recently, rapid progress in imaging methods have provided such spatially resolved *multi-point* measurements, that the mandatory information one needs to generate instantaneous vector fields has become available.

The velocity field $\vec{u}(x, y, z, t)$ is a vector function of space and time. At present, none of the modern techniques are capable of electronically recording such a data field completely (i.e. with sufficient resolution in all dimensions) except for some special cases (e.g. slow flows). The reason for this deficiency is the huge amounts of data produced. As a result

all techniques today make some compromise through the limiting of spatial or temporal resolution.

For clarity a distinction must be made between measurements in a recording plane ('planar velocimetry') and measurements extracted directly from a fluid volume ('volume velocimetry') - not to be confused with the common labels of '2D' and '3D' velocimetry which refer to the number of simultaneously acquired velocity vector components.

B.1 Planar Particle Imaging Velocimetry (PIV)

The deficiencies of straightforward particle tracking algorithms (trying to follow features which are virtually indistinguishable from their neighbours) has led to the idea of tracking not the particle images themselves but *constellations of particles* which should be much more distinguishable due to their spatial arrangement. As long as the local velocity field is reasonably smooth the constellations should displace as a whole and without internal distortions.

The non-intrusive method (shown in Figure 15) makes use of a laser beam stretched into a plane which illuminates the flow field seeded with tiny neutrally buoyant particles - so called 'tracers'.

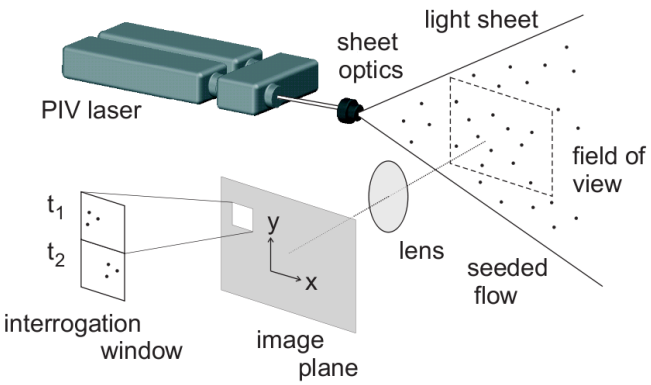

Figure 15: General setup of a 2D PIV measurement. [7]

From sequentially recorded images the 2D velocity can be derived with the ratio,

$$\vec{u} = \frac{\triangle(x, y)}{\triangle t}. \tag{10}$$

It turns out that the particle constellations are so unique that usually only two exposures are necessary to identify corresponding patterns. This idea is then implemented to sub-windows (so called 'interrogation windows' containing the distinguishable particle constellations) of the two recorded images by means of the *cross-correlation* method; proven to be the fastest through computational implementation of the Fast Fourier Transform (FFT).

The challenge for the user becomes one of selecting a suitable time difference, spatial resolution and, after image acquisition, the appropriate interrogation window for the cross-correlation algorithm, illustrated with an example in Figure 16.

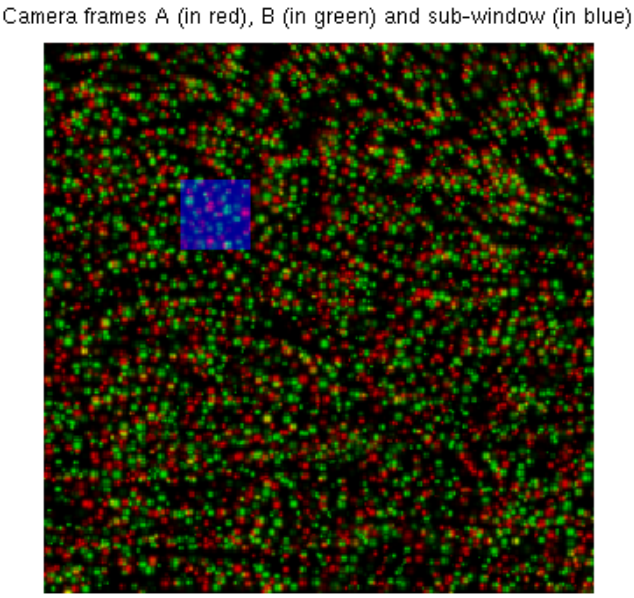

Figure 16: Temporally separated camera frames A and B showing differing particle displacement throughout the image and a sub-window of 32×32 pixels selected for constant-constellation movement.

Results in Figure 17 of the cross-correlation from this example show the most 'likely' displacement vector from frame A to frame B through the highest probability peak. Performing this cross-correlation for each sub-window gives us the vector map illustrated in Figure 18 which serves as a disparity map between the two frames.

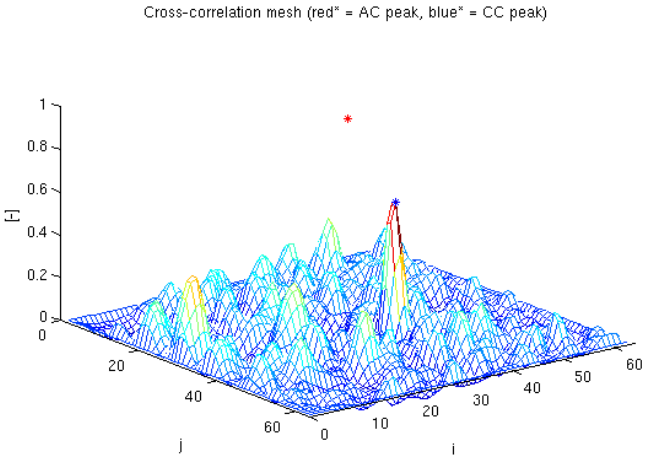

Figure 17: Cross correlation from frame A to frame B showing possible displacement between them on $[\delta x, \delta y] = \pm 32$ with a probability peak.

One solution for obtaining the third vector component is the utilisation of Stereo PIV.

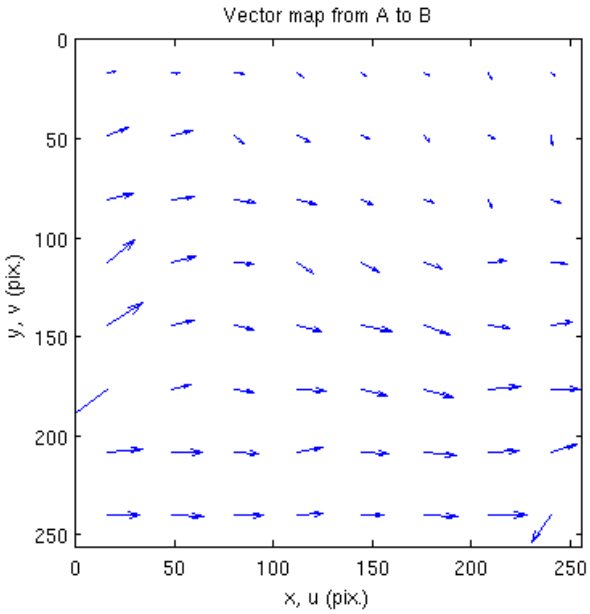

Figure 18: Vector map from frame A to frame B (note the two *erroneous* vectors resulting from misleading cross-correlation peaks) - Postprocessing can take care of these minor blemishes

If the light sheet of a 'standard' PIV setup is made thick enough then a high-resolution CCD camera can also resolve a particle's motion across the sheet. If two cameras look at the same light sheet with a known offset angle (parallax), the out-of-plane component of the velocity field can be computed through a simple triangulation step.

C Fluorescence Techniques

Many of the fluorophores used in Imaging Flow Diagnostics are toxic - can cause irritation to skin and eyes and should always be disposed of responsibly.

Fluorescence is a three-step process which occurs in certain molecules called fluorophores or fluorescent dyes. The first, *excitation*, is the absorption of a photon hn_{ex} by the fluorophore. In the second step, the *excited state* (which exists for a finite time; $10^{-9} - 10^{-8}$ seconds), the fluorophore undergoes configurational changes and interactions with its molecular environment. The processes involved have two important consequences; that of dissipating the energy towards the fluorescence emission, and that of colliding (quenching) with neighbouring molecules, i.e. not all excited fluorophores return to the ground state. In the third step, the *fluorescence emission*, a photon hn_{em} is emitted, returning the fluorophore to its ground state. Due to the energy dissipation during the excited-state lifetime, the energy of this returned photon is lower and therefor of longer wavelength than that of the excitation photon. The process is different from chemiluminescence in which the excited state is created by the energy excess of a chemical reaction.

The difference in energy or wavelength represented by $hn_{ex} - hn_{em}$ is called the Stokes

shift.The entire fluorescence process is cyclical and, unless the fluorophore is irreversibly destroyed in the excited state (a phenomenon known as photo-bleaching), the same fluorophore can be repeatedly excited and its emission detected.

The fluorescence signal produced by weak laser pumping may be described by a linear relationship, dependent on the excitation wavelength λ and the temperature T,

$$F_f(\lambda, T) = \eta_{opt} \frac{\Omega}{4\pi} \frac{E_{las}}{\frac{hc}{\lambda}} dV_c \times n_{abs}(T)\sigma(\lambda, T)\phi(\lambda, T). \tag{11}$$

In this formula:

$$\begin{aligned}
h_{opt} &= \text{optical collection efficiency,} \\
\frac{\Omega}{4\pi} &= \text{solid angle of the collection optics,} \\
E_{las} &= \text{laser energy,} \\
\frac{hc}{\lambda} &= \text{energy of an excitation photon,} \\
dV_c &= \text{excited spatial volume,} \\
n_{abs}(T) &= \text{number density of absorbing molecules,} \\
\sigma(\lambda, T) &= \text{absorption cross section of the fluorescent molecules, and} \\
\phi(\lambda, T) &= \text{the fluorescence quantum yield.}
\end{aligned}$$

The dependence on pressure, notably the quenching effects (e.g. from O_2), are implicitly captured in the absorption cross section and quantum yield. In general, the effect of quenching leads to a reduction in the fluorescence signal of the form by a factor $\frac{A}{A+Q}$, where A is the spontaneous (luminous) emission rate and Q the (non-radiative) quenching rate.

The fluorescence equation points to the different ways in which the fluorescence effect can be used. The linear dependence of the fluorescence signal S_f on the number density n_{abs} of fluorophores (or the concentration of a suitable dye) can be used to determine the density of the dye tracer material. For this the fluid will normally have to be isothermal and pressure effects should also be negligible. Conversely, if the number density is held constant (uniform seeding), the temperature can be measured following a suitable calibration of the fluorescence response.

If the spontaneous emission and quenching rates of the fluorescence signal can be explicitly analysed, one obtains methods capable of measuring temperature and pressure simultaneous.

C.1 Concentration measurements with PLIF

Planar Laser Induced Fluorescence (PLIF) is by now a widely used technique to visualise species concentrations and to quantify mixing phenomena. In a 'generic' setup, the fluorescent dye is uniformly mixed together with a host fluid. This fluorescent mixture is then used in the flow experiment where it normally interacts with another, non-fluorescent fluid volume. As a consequence, the strength of the fluorescence signal at any given time indicates the local concentration of dyed fluid or its degree of dilution (see Figure 19).

Figure 19: Example of LIF measurement in mixing concentrations. [16]

C.2 Temperature measurements with PLIF

If one can ensure that the flow to be analysed is seeded homogeneously (uniform density and pressure), the brightness of the fluorescence signal can be processed to give temperature. For this one makes use of the temperature and pumping wavelength dependence of the fluorescence.

D The Exergy of Stratified Thermal Energy Storages

Inspired by the work of [4], [14], [15] and [5] the entropy and exery of the TES investigated was balanced using the change in energy between states in which the TES was found.

The energy E and exergy Ξ in the TES can be found by integrating over the entire storage-fluid mass m within the TES as follows:

$$E = \int_m e \ dm \tag{12}$$

$$\Xi = \int_m \xi \ dm \tag{13}$$

where e denotes specific energy and ξ specific exergy. For an ideal liquid e and ξ are functions of temperature only and can be expressed using

$$e(T) = c(T - T_0) \tag{14}$$

$$\begin{aligned} \xi(T) &= c\left[(T - T_0) - T_0 \ln\left(\frac{T}{T_0}\right)\right] \\ &= e(T) - cT_0 \ln\left(\frac{T}{T_0}\right) \end{aligned} \tag{15}$$

where the reference temperature (the temperature against which the quality of the TES's energy is measured; inlet or room temperature) T_0 is assumed constant and c is a function of temperature.

Considering now the height H of the TES which exhibits stratification in the vertical dimension where a horizontal element of mass dm can be approximated with

$$\mathrm{d}m = \frac{m}{H}\mathrm{d}z, \tag{16}$$

thence onwards expressions for e and ξ can be written as

$$e(z) = c(T(z) - T_0) \tag{17}$$

$$\xi(z) = e(z) - cT_0 \ln\left(\frac{T(z)}{T_0}\right) \tag{18}$$

and be substituted back into Eqs. (12) and (13) respectively to give

$$E = \frac{m}{H}\int_0^H e(z)\mathrm{d}z \tag{19}$$

$$\Xi = \frac{m}{H}\int_0^H \xi(z)\mathrm{d}z \tag{20}$$

Measurements were performed using ten Pt100 (Platinum resistive temperature 100Ω) sensors distributed over the vertical length of the water column (see Figure 20).

Observing the temperature distribution of the tank as a continuous linear distribution between sensors gives nine horizontal zones in which the temperature in each varies linearly from the bottom to the top, expressed as

$$T(h) = \begin{cases} \vartheta_1(z), & z_0 \le z \le z_1 \\ \vartheta_2(z), & z_1 \le z \le z_2 \\ \cdots & \\ \vartheta_9(z), & z_8 \le z \le z_9 \end{cases} \tag{21}$$

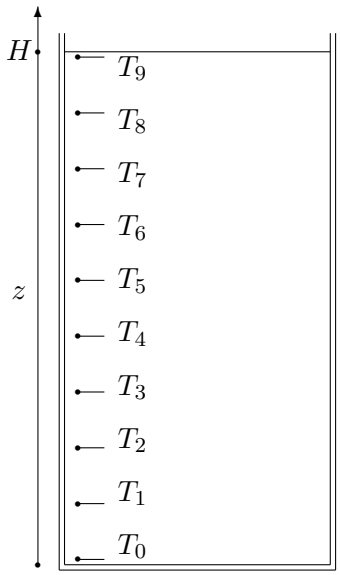

Figure 20: TES Temperature measurements

where $\vartheta_j(z)$ represents the height dependent linear temperature distribution in zone j found using

$$\vartheta_j(z) = \frac{T_j - T_{j-1}}{z_j - z_{j-1}} z + \frac{z_j T_{j-1} - z_{j-1} T_j}{z_j - z_{j-1}} \tag{22}$$

given

$$0 \approx z_0 \leq z_1 \leq z_2 \leq \cdots \leq z_9 \approx H. \tag{23}$$

For the purpose of weighting these zones we introduce x_j, the mass fraction for zone j:

$$x_j \equiv \frac{m_j}{m} \tag{24}$$

which, given the assumption that the horizontal cross-sectional area and the TES fluid section densities are constant and the vertical thickness of each zone j can vary in thickness, simplifies to

$$x_j = \frac{z_j - z_{j-1}}{H}. \tag{25}$$

The mean temperature of the TES which we also refer to with T_{tes} can be approximated with

$$T_m = \sum_{j=1}^{9} x_j (T_m)_j \tag{26}$$

where $(T_m)_j$ is the mean temperature in zone j and was used in the calculations for entropy generation in each horizontal layer of the tank:

$$(T_m)_j = \frac{T_j + T_{j-1}}{2}. \tag{27}$$

References

[1] Ali, M. E. Experimental investigation of natural convection from vertical helical coiled tubes. *Int. Journal of Heat Mass Transfer 37*, 4 (1994), 665–671.

[2] Farrington, R. B., and Bingham, C. E. Testing and analysis of immersed heat exchangers. Tech. Rep. 254-2866, Solar Energy Research Institute (now National Renewable Energy Laboratory), 1986.

[3] Frank, E., Luzzi, A., and Logie, W. Strömungsuntersuchungen an Schichtspeichern und Wärmetauscher - Jahresbericht 2007. Tech. rep., Institut für Solartechnik SPF, 2007.

[4] Hahne, E., Kübler, R., and Kallweit, J. The evaluation of thermal stratification by exergy. In *Energy Storage Systems* (1989), Kluwer Academic Publishers, pp. 465–485.

[5] Huhn, R. *Beitrag zur Thermodynamischen Analyse und Berwertung von Wasserwärmespeichern in Energieumwandlungsketten.* PhD thesis, Technischen Universität Dresden, 2007.

[6] Krishne Gowda, Y. T., Aswatha Narayana, P. A., and Seetharamu, K. N. Numerical investigations of mixed convection heat transfer past an in-line bundle of cylinders. *Journal of Heat and Mass Transfer 41*, 11 (1997), 1613–1619.

[7] Lavision GmbH. *Product Manual: Flowmaster.* Anna-Vandenhoeck-Ring 19, D-37081 Göttingen, Dec 2007. www.lavision.de.

[8] Messerschmid, H. *Entwicklung und Validation eines numerischen Verfahrens zur Beurteilung von Trinkwasserspeichern.* PhD thesis, Universtität Stuttgart, Lehrstuhl für Heiz- und Raumlufttechnik, 2002.

[9] Morgan, V. T. The overall convective heat transfer from smooth circular cylinders. In *Advances in Heat Transfer* (New York, 1975), vol. 11, Academic Press Inc., pp. 199–264.

[10] Morrison, G. L., Rosengarten, G., and Behnia, M. Mantle heat exchangers for solar horizontal tank thermosyphon solar heat heater. *Solar Energy 67*, 1–3 (1999), 53–64.

[11] Mote, R., and Probert, S. D. The performance of a coiled finned-tube heat exchanger submerged in a hot water store: the effect of the exchangers orientation. *Applied Energy 38*, 1–19 (1991).

[12] Prabhanjan, D. G., Rennie, T. J., and Vijaya Raghavan, G. S. Natural convection heat transfer from helical coiled tubes. *Int. Journal of Thermal Sciences 43* (2003), 359–365.

[13] Raithby, G. D., and Hollands, K. G. T. A general method of obtaining approximate solutions to laminar and turbulent free convection problems. In *Advances in Heat Transfer* (New York, 1975), vol. 11, Academic Press Inc., pp. 265–315.

[14] Rosen, M. A. The exergy of stratified thermal energy storages. *Solar Energy 71*, 3 (2001), 173–185.

[15] Rosengarten, G., Morrison, G., and Behnia, M. A second law approach to characterising thermally stratified hot water storage with application to solar hot water. *ASME Journal of Solar Energy Engineering 121* (1999), 194–200.

[16] Rösgen, T. *Quantitative Flow Visualisation*, 1.4.2 ed. Institut für Fluiddynamik, ETH Zürich, 2002. Lecture script.

[17] Shah, L. J., and Furbo, S. Correlation of experimental and theoretical heat transfer mantle tanks used in low flow sdhw systems. *Solar Energy 64*, 4–6 (1998), 245–256.

[18] Su, Y., and Davidson, J. H. Natural convective flow and heat transfer in a collector storage with an immersed heat exchanger: numerical study. *ASME Journal of Solar Energy Engineering 127* (2005), 324–332.

[19] Su, Y., and Davidson, J. H. Transient natural convection heat transfer correlations for tube bundles immersed in a thermal storage. *ASME Journal of Solar Energy Engineering 129* (2007), 210–214.

[20] van Koppen, C. W. J., Thomas, J. P. S., and Veltkamp, W. B. The actual benefits of thermally-stratified storage in a small and medium size solar system. In *Proceedings of ISES Solar World Congress* (Atlanta, 1979), pp. 579–580.

[21] Xin, R. C., and Ebadian, M. A. Natural convection heat transfer from helicoidal pipes. *Journal of Thermophysics and Heat Transfer 10*, 2 (1996), 297–302.